Supporting Information

Liu et al. 10.1073/pnas.1220689110

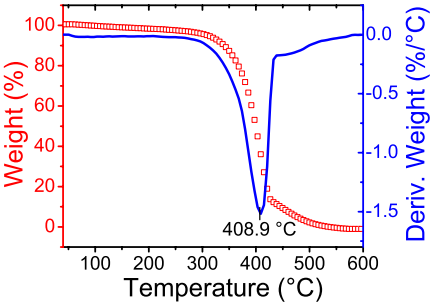

Fig. S1. Thermogravimetric analysis of poly(ethylene oxide)-*block*-poly(2-vinyl pyridine) (PEO-*b*-P2VP). The thermal decomposition peak of PEO-*b*-P2VP is at 409 °C. The temperature ramping rate, 10 °C·min^{-1}.

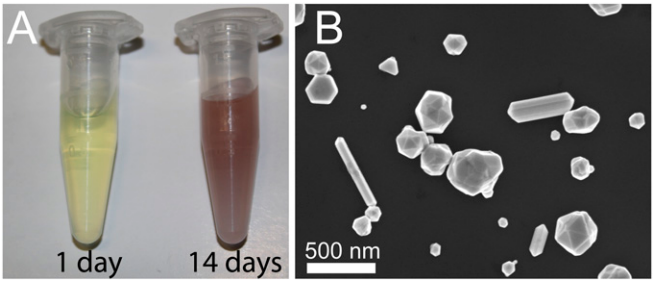

Fig. S2. Reduction of Au^{III} at room temperature. (*A*) Photograph of $HAuCl_4$ in PEO-*b*-P2VP aqueous solution (Au^{III}:2VP = 4:1) after 1 and 14 d. After 1 d, the Au^{III} is not yet reduced, exhibiting a yellowish color. After 14 d, the color of the solution changed to red, indicating the reduction of Au^{III} to Au^0 and the formation of Au nanoparticles in solution. We choose the ratio of Au:2VP = 4:1 to highlight the color change. (*B*) Scanning EM image of representative Au nanoparticles formed in the solution after 14 d. Note that the nanoparticles have various sizes and shapes. Because Au and Ag have the highest reduction potential among the precursors used, to minimize the precursor reduction under ambient conditions before nanoparticle synthesis, the Au and Ag inks are used within 3 d of preparation.

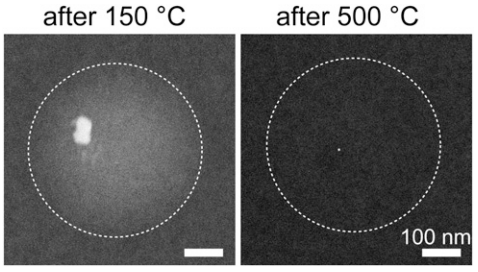

Fig. S3. High-angle annular dark-field scanning transmission EM (TEM; *Z* contrast) images showing the stages of Pt nanoparticle formation. After annealing at 150 °C (*Left*), the precursor, H_2PtCl_6, aggregated within the polymer nanoreactor. After annealing at 500 °C (*Right*), the precursor decomposed and formed a single nanoparticle. The polymer nanoreactors were also decomposed. The dashed circles outline the boundary of the polymer nanoreactors.

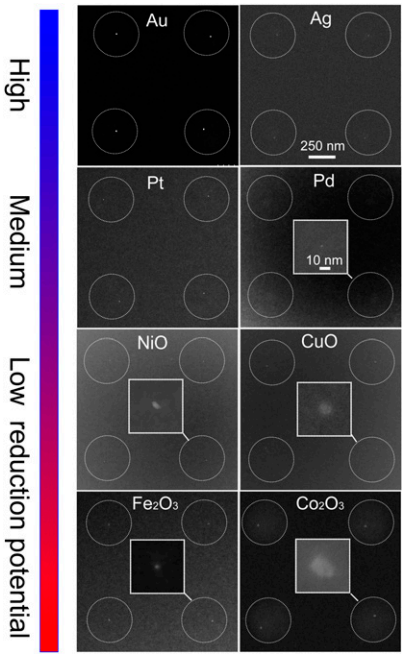

Fig. S4. Representative STEM images of arrays of various nanoparticles. Dotted circles highlight the position of nanoparticles as a guide to the eye. The contrast of the elements with low atomic number is not clear in the low-magnification images. For clarity, zoomed-in images of nanoparticles are shown in *Insets*. The scale bars apply to all panels and *Insets*. Note that the different sizes of the nanoparticles are determined by the ink concentration and the amount of polymer delivered to the synthesis sites.

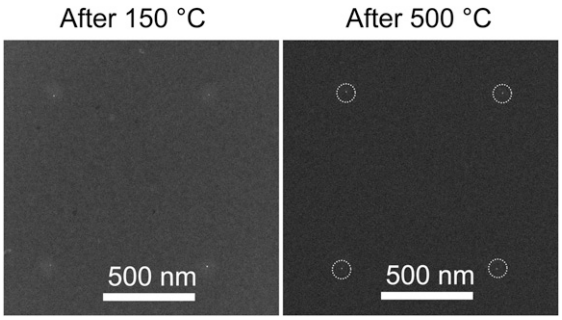

Fig. S5. STEM images showing the stages of Ag nanoparticle formation. A patterned array of PEO-*b*-P2VP nanoreactors on hydrophobic silicon nitride window after the first annealing step at 150 °C (*Left*) and after the second annealing step at 500 °C (*Right*). Ag nanoparticles were observed after the first annealing step. Dotted circles denote the position of the patterned polymer spots.

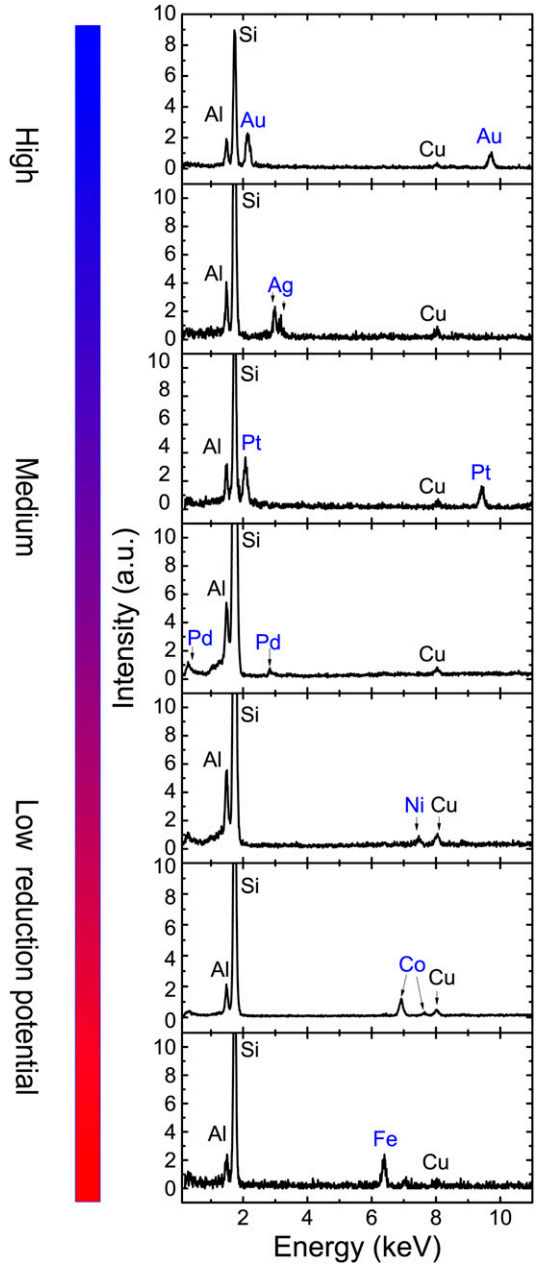

Fig. S6. Energy-dispersive X-ray spectra of the synthesized metal nanoparticles. Si signal is from the silicon nitride membrane. Al and Cu signals are from the TEM sample holder. Because a Cu signal is always present in the background, an energy-dispersive X-ray spectroscopy spectrum of Cu-containing nanoparticles is not shown.

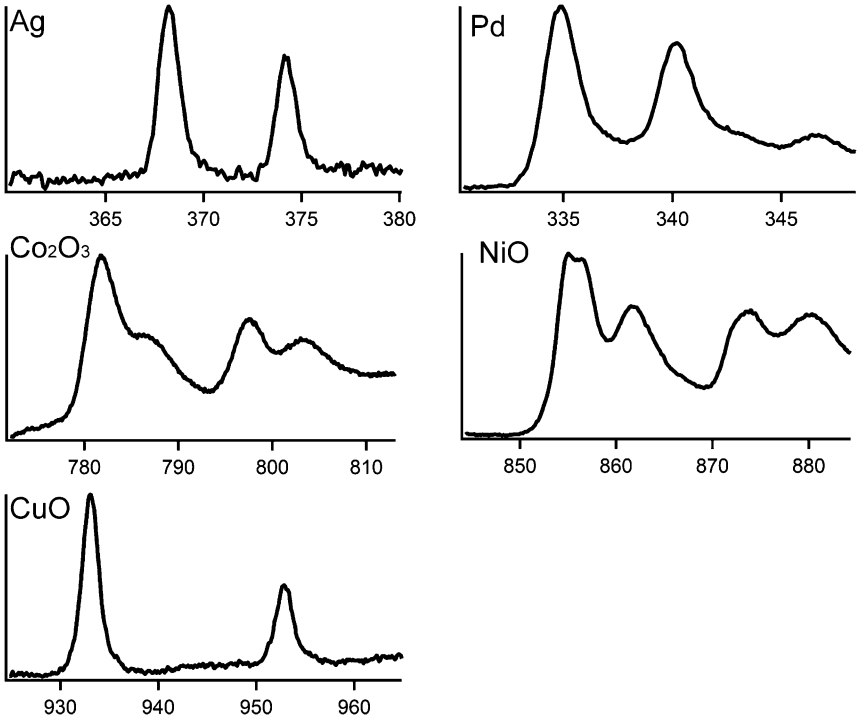

Fig. S7. X-ray photoelectron spectroscopy spectra of nanoparticles composed of Ag, Pd, Co_2O_3, NiO, and CuO. All spectra shown here are for nanoparticles at the end of the synthesis process (that is, after sequential annealing at T_{low} and T_{high}). All core element peak positions (except CuO) fall within the expected range for the listed compositions, and all compositions are corroborated with results from high-resolution TEM. The one exception is the high-resolution Cu scan, which shows mostly Cu^{I}; this finding is in contrast to the high-resolution TEM results, which indicate that the nanoparticles are CuO (and hence, Cu^{II}). This discrepancy is caused by in situ reduction of Cu^{II} to Cu^{I}, which has been observed by others (1).

1. Chusuei CC, Brookshier MA, Goodman DW (1999) Correlation of relative X-ray photoelectron spectroscopy shake-up intensity with CuO particle size. *Langmuir* 15(8):2806–2808.

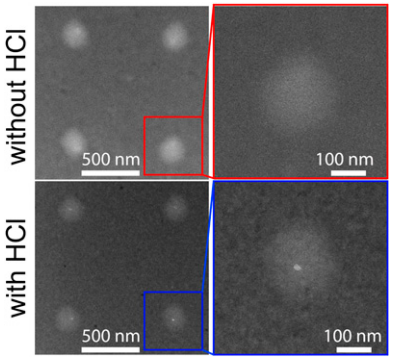

Fig. S8. Effect of protonation of PEO-*b*-P2VP on the loading of precursors. STEM images of patterned arrays of nanoreactors of PEO-*b*-P2VP on a silicon nitride window after the first annealing step at 150 °C. Phase separation of Na_2PdCl_4 is only observed when HCl is mixed in the aqueous solution of PEO-*b*-P2VP.

Table S1. Standard reduction potential of the materials used

Half reaction	..... E° (volts)
$AuCl_4^-(aq) + 3e^- \rightarrow Au(s) + 4Cl^-(aq)$	..... E° = 1.002
$Ag^+ + e^- \rightarrow Ag(s)$	..... E° = 0.7996
$[PtCl_4]^{2-}(aq) + 2e^- \rightarrow Pt(s) + 4Cl^-(aq)$	..... E° = 0.755
$[PtCl_6]^{2-}(aq) + 2e^- \rightarrow [PtCl_4]^{2-}(aq) + 2Cl^-(aq)$	..... E° = 0.68
$[PdCl_4]^{2-}(aq) + 2e^- \rightarrow Pd(s) + 4Cl^-(aq)$	..... E° = 0.591
$Cu^{2+} + 2e^- \rightarrow Cu(s)$	..... E° = 0.3419
$2H^+ + 2e^- \rightarrow H_2(g)$	..... E° = 0.00000
$Fe^{3+} + 3e^- \rightarrow Fe(s)$	..... E° = −0.037
$Ni^{2+} + 2e^- \rightarrow Ni(s)$	..... E° = −0.257
$Co^{2+} + 2e^- \rightarrow Co(s)$	..... E° = −0.28

Data from ref. 1.

1. Haynes WM, ed (2011) *CRC Handbook of Chemistry and Physics* (CRC, Boca Raton, FL), 92nd Ed.

Table S2. Decomposition of the metal precursors used

Precursor	Decomposition temperature (°C)	Decomposition pathway	Refs
H_2PtCl_6	~220–510	$H_2PtCl_6 \rightarrow PtCl_4 \rightarrow PtCl_{3.5} \rightarrow PtCl_2 \rightarrow Pt$	1
$AgNO_3$	~285–415	$AgNO_3 \rightarrow Ag$	2
$Fe(NO_3)_3{\cdot}9H_2O$	~156	$Fe(NO_3)_3{\cdot}9H_2O \rightarrow Fe(OH)(NO_3)_2 \rightarrow Fe(OH)_2NO_3 \rightarrow FeOOH \rightarrow \alpha\text{-}Fe_2O_3$	2, 3
$Co(NO_3)_2{\cdot}6H_2O$	~180	$Co(NO_3)_3{\cdot}6H_2O \rightarrow Co(NO_3)_3{\cdot}4H_2O \rightarrow Co(NO_3)_2 \rightarrow Co_2O_3$	2, 4
$Ni(NO_3)_2{\cdot}6H_2O$	~250–300	$Ni(NO_3)_2{\cdot}6H_2O \rightarrow Ni(NO_3)_2{\cdot}2H_2O \rightarrow Ni(NO_3)(OH)_2{\cdot}H_2O \rightarrow Ni(NO_3)(OH)_{1.5}O_{0.25}{\cdot}H_2O \rightarrow Ni_2O_3 \rightarrow Ni_3O_4 \rightarrow NiO$	4
$Cu(NO_3)_2{\cdot}3H_2O$	~200–250	$Cu(NO_3)_2{\cdot}3H_2O \rightarrow Cu_2(OH)_3NO_3 \rightarrow CuO$	2, 5

1. Schweizer E, Kerr GT (1978) *Inorg Chem* 17(8):2326–2327.
2. Mu J, Perlmutter DD (1982) *Thermochim Acta* 56(3):253–260.
3. Wieczoreck-Ciurowa K, Kozak A (1999) *J Therm Anal Calorim* 58(3):647–651.
4. Brockner W, et al. (2007) *Thermochim Acta* 456(1):64–68.
5. Morozov IV, et al. (2003) *Thermochim Acta* 403(2):173–179.